TECHNICAL REPORT: MODEL SENSITIVITY TO SURFACE TOPOGRAPHY

ESTEC Contract 11369/95/NL/JG

S. R. Lewis, M. Collins and P. L. Read

January 20, 1998

Contents

1 Introduction

This document describes a series of sensitivity runs with the AOPP version of the Mars Global Circulation Model to assess the model sensitivity to uncertain features of the 'boundary conditions'. One of the largest uncertainties in the model comes with the prescribing of the surface topographic height, of which there are various data sets currently available. It is the main aim of this report to assess the model sensitivity with respect to the surface topography with particular emphasis on any differences which may be important in the engineering design of future Mars missions.

2 Topographic Data

The surface topography is one of the most impressive features of the planet Mars. It shows a marked north-south asymmetry, the heavily cratered southern hemisphere being higher on average relative to the mean geoid than the younger northern hemisphere. The Tharsis plateau dominates the surrounding reference surface, by more than 8 km, and extends over about one fourth of the longitudinal domain in equatorial regions. The largest shield volcanos are particularly impressive, culminating in altitudes of up to 25 km. The huge canyon Valles Marineris is more than 4000 km long and about 500 km wide. Despite the fact that Mars is a smaller planet than the Earth, its topography is of a greater scale, both in the horizontal and vertical. Since both atmospheres have similar pressure scale heights (about 10 km in the case of Mars and slightly less for Earth), it is to be expected that the surface topography of Mars is an important influence on the atmospheric circulation.

The elevations mentioned here are referenced to the zero elevation reference surface as outlined in [11]. This is a gravity level surface described in terms of spherical harmonics of fourth degree and fourth order combined with a 610 Pa mean pressure surface with a mean radius of 3382 km.

2.1 Current Topographic Maps

Although the main features of the martian surface have been extensively surveyed, largely by the Viking orbiter cameras, the accurate determination of the martian topography is still remarkably controversial. Three datasets representing the surface topography are currently available:

Consortium: The first topographic dataset (fig. 1) was derived from the Mariner 9 radio occultations and gravity field measurements [5, 8]. It has a theoretical accuracy of about 1 km relative to the mean geoid, and a reasonable horizontal resolution (it is available on a 1 degree grid, but is relatively smooth at this scale). The main weakness of the consortium dataset is the absence of coverage in the polar regions, particularly in the southern hemisphere, poleward of about 60°S.

Digital Topographic Map (DTM): The DTM (fig. 2) was derived completely independently of the Consortium dataset by digitizing contour levels of a map which was constructed using a variety of data, including the stereographic imaging of the surface by the Viking orbiters [10]. Although this dataset accounts well for fine structures not visible in the Consortium dataset (it is available at resolutions of up to 64 pixels per degree), it seems to suffer from substantial biases on larger scales. For instance, the location of the landing site of Viking 2 in the DTM is at a higher altitude than that of Viking 1, although Viking 2 is generally believed to lie about 1 km below Viking 1, an altitude difference derived from the observed annual mean atmospheric pressure differences between the two sites.

Zuber-Smith: This, the most recent dataset, was constructed by using only the Viking radio occultations and the estimated altitude difference between the two Viking landing sites. This dataset has a very low horizontal resolution, though it is thought to have some desirable properties on the very largest, planetary scales. See fig. 3 for a comparison of the three datasets degraded to a similar low resolution.

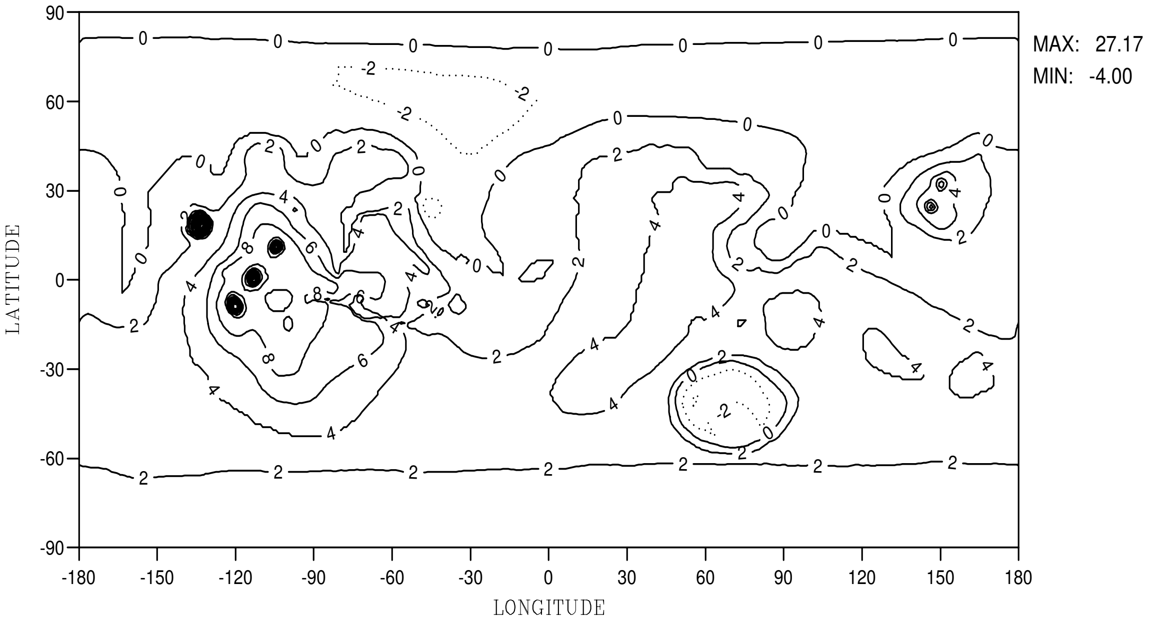

Figure 1: The surface altitude of Mars (km) from the Consortium dataset. Contour interval 2km, negative contours are dashed.

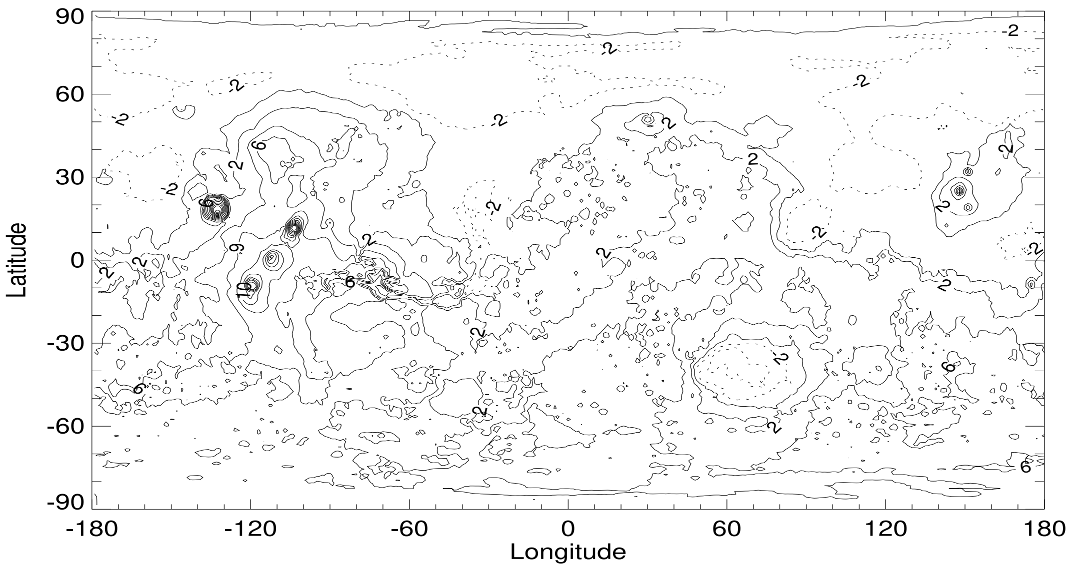

Figure 2: The surface altitude of Mars (km) from the DTM dataset. Contour interval 2km, negative contours are dashed.

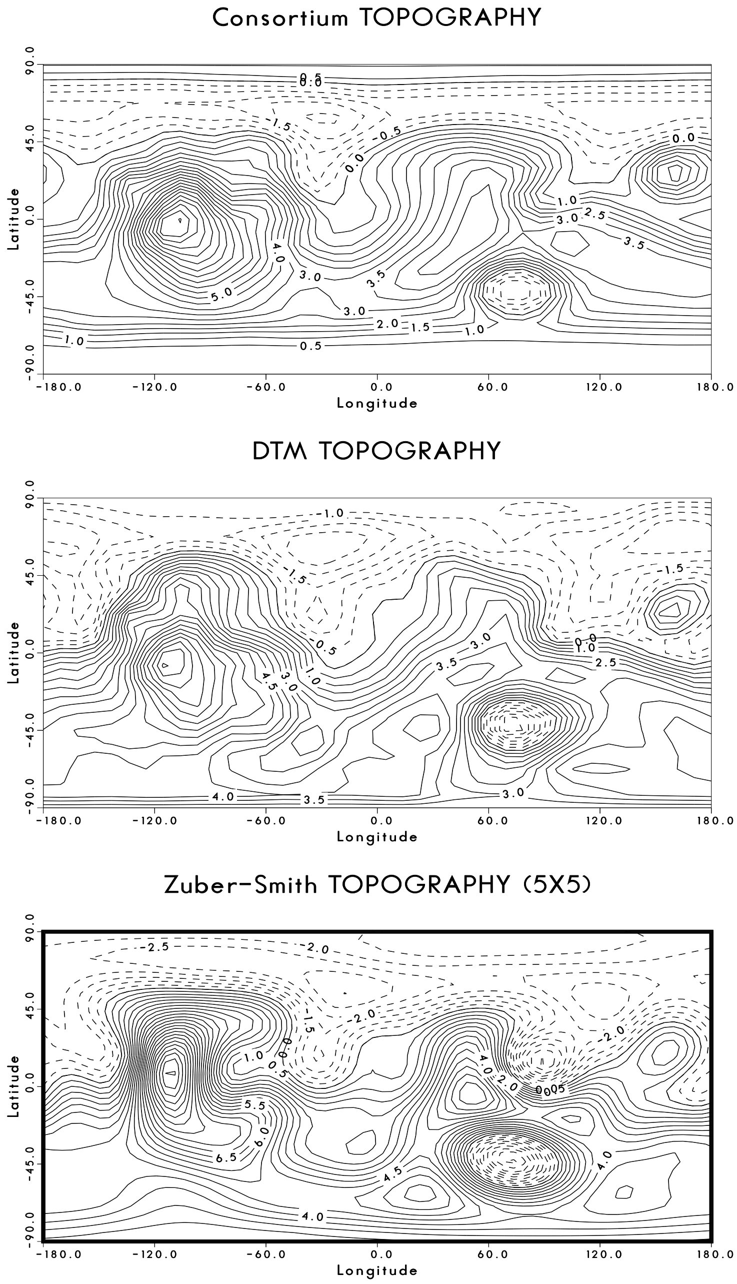

Figure 3: Comparison of the three topography datasets available: (top) consortium, (middle) DTM, and (low) Viking radio-occultations. The three dataset have been smoothed to the same very low horizontal resolution.

2.2 Comparison of DTM and Consortium Topography

The DTM data was chosen for the main set of model runs that were used to compile the Mars Climate Database [2, 4]. This was possibly one of the hardest choices to make during the project as there are strong and conflicting arguments for using both the DTM and the Consortium sets; the horizontal resolution of the Zuber-Smith dataset is much lower than that of the Mars climate models and it was consequently ruled out. The DTM was chosen for its complete global coverage and small-scale detail, which is an important input parameter for the gravity wave and form drag scheme [3], though the possibility of large-scale biases in the mean topography is a concern. The main aim of this report is to assess the sensitivity of the model climate to the differences between the DTM and Consortium data.

Figure 4 shows both the DTM and the Consortium topography at the resolution of the Mars Climate Database and as used in the model. This is not merely a process of sampling the full datasets on the database grid, but also involves some smoothing to the full resolution of the model in Fourier space. Figure 4 also shows a difference map. Perhaps the most striking difference is in the southern hemisphere polar region where the DTM is consistently around 5 km higher than the Consortium, but there is also a large region of up to 5 km differences in the northern hemisphere at longitudes between 120°W and 80°W, where the DTM extends the northern range of the Tharsis ridge significantly. Over much of the planet differences are at least 1 km and often 2–3 km. It is therefore clear that the mean surface pressure at most sites will differ by a large amount between models run with the two different topographies and the large scale differences, such as the higher southern polar region and more strongly zonal wavenumber two nature of the topography in northern mid-latitudes in the DTM may have profound effects upon the global atmospheric circulation.

Figure 5 shows the sub-grid-scale standard deviation for each topographic dataset and the difference between them. The sub-grid-scale standard deviation is a measure of the variation of the topography which is not explicitly resolved around each model grid-point. This field is an important input parameter to the gravity wave and low-level form drag

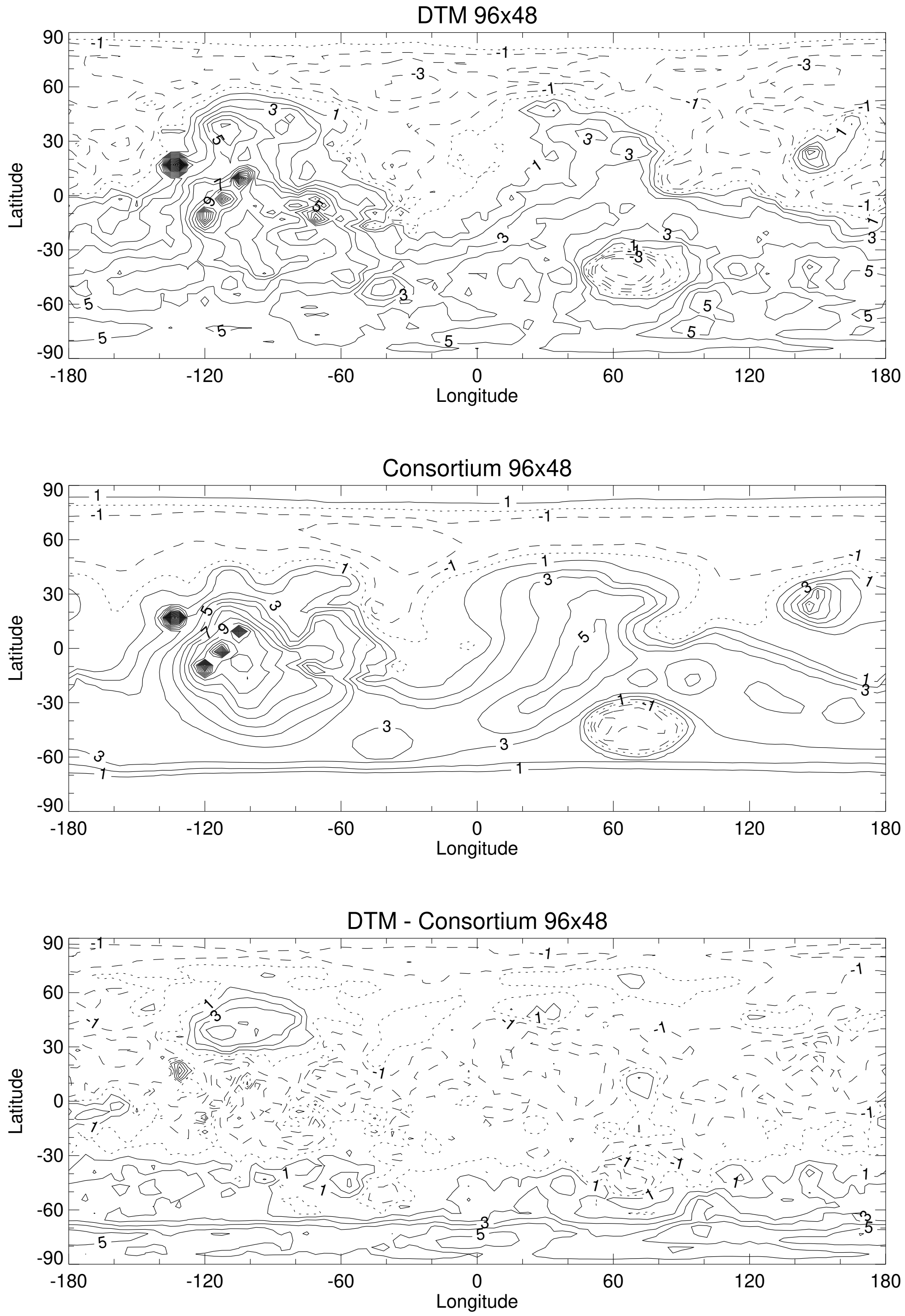

Figure 4: Comparison of the DTM and Consortium datasets at the resolution of the Mars Climate Database, with the difference between the datasets shown in the third frame. Contour interval 1km, zero contour is dotted, negative contours are dashed.

schemes [3], measuring the effective roughness of the terrain which would have an impact on these parameterized processes. It is clear that the DTM is rougher on small scales, especially in the southern hemisphere, as expected. The Consortium, in contrast, only shows strong sub-grid-scale variance around the major volcanos, Valles Marineris and the edge of the Hellas basin, as well as a rather artificial band close to 70°S where the topographic data has come to an end. In the region 60°S to 70°S the topographic height falls rapidly to zero, corresponding to the 'cliff' visible in the mean data (figure 4, second frame).

Figure 6 shows the anisotropy fields, a measure of the ratio of the sub-grid-scale standard deviation along the principal axes of the topography; these are aligned with the direction of maximum and minimum gradient around each grid-point. A value of zero implies no variance in one direction, e.g. a flat slope, and a value of one implies equal variance in all directions. This field also forms an input to the sub-grid-scale parameterization routines [3]. Once again, it is clear that the DTM is much rougher and less coherent on scales smaller than the martian models used to form the database are able resolve, whereas the Consortium data is very smooth on small scales. Such small-scale roughness in the DTM is probably more realistic, indicating the advantage of using the DTM when sub-grid-scale fields are required for parameterizations.

3 Studies of Sensitivity to Surface Topography

Various experiments to study the sensitivity of the modelled martian climate to topography have been performed. In this document we concentrate on a pair of experiments using the Oxford martian general circulation model; to be consistent exactly the same form of the Oxford model was used for each experiment as was used to compile version 1.0 of the Mars Climate Database and a few minor corrections and improvements which have since been made [7] were not used. The first experiment is one year of the standard Viking dust scenario (a model run used to compile version 1.0 of the Mars Climate Database, which covers dust optical depths from 0.4 to 1.0) and the second is

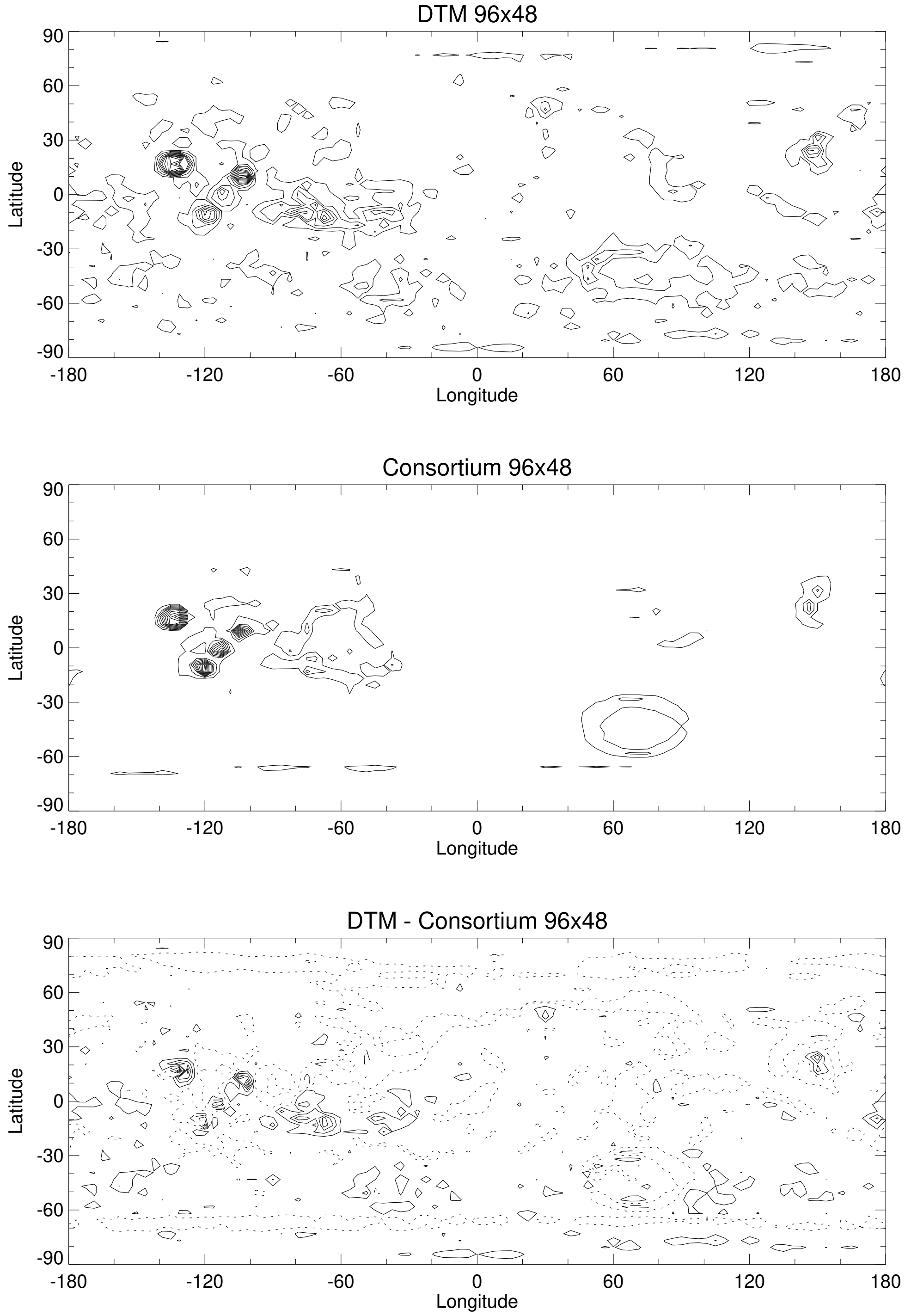

Figure 5: Comparison of the DTM and Consortium sub-grid-scale standard deviation at the resolution of the Mars Climate Database, with the difference shown in the third frame. Contour interval 500m.

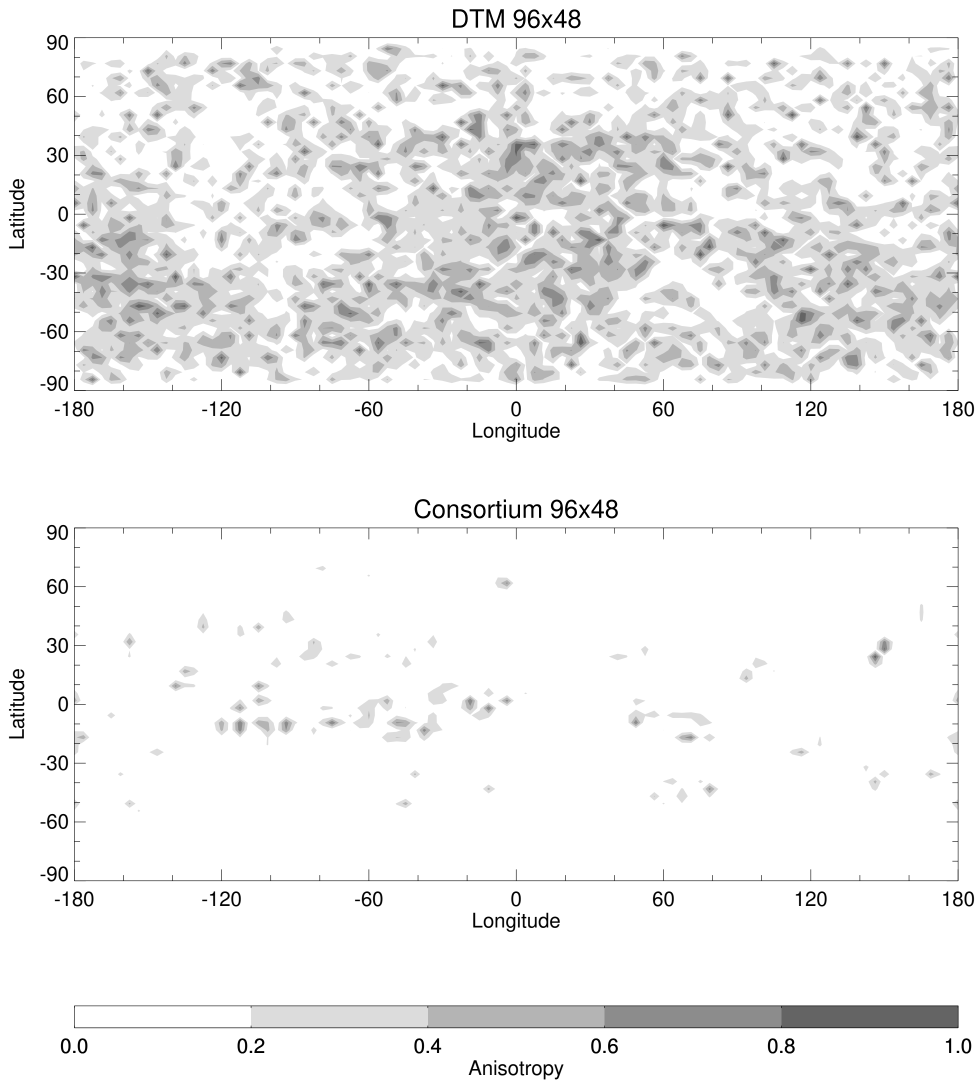

Figure 6: Comparison of the DTM and Consortium sub-grid-scale anisotropy at the resolution of the Mars Climate Database.

a run with the same parameters except that the Consortium topographic dataset was used at the lower boundary of the model. For brevity we choose to compare the models over three seasonal periods, covering both solstices and one equinox: $L_s = 90° - 120°$ (northern hemisphere summer), $L_s = 180° - 210°$ (northern hemisphere autumn) and $L_s = 270° - 300°$ (northern hemisphere winter).

The results of these experiments are surveyed below, first describing the zonal and time mean circulations and then comparing the main forms of variability within each experiment in order of decreasing magnitude. Finally, some typical profiles are extracted from each experiment, as they might be from a climate database compiled from the results.

3.1 Zonal-Mean Circulation

It is first useful to compare the gross statistics of the DTM and Consortium runs to assess whether there is any major sensitivity to the surface topography. Figures 7–9 show the zonal mean temperature, zonal wind and meridional wind from the two runs during three seasons. While the circulation features are in broadly good agreement, indicating no extreme sensitivity to surface topography, there is one significant difference in the fields. Note the slight difference in shape of the winter westerly jet in the southern hemisphere during the northern summer period (figure 7). This corresponds to differences in the south pole upper level temperature structure, where there is more dynamical warming in the DTM case, resulting in a stronger temperature inversion over the pole. As described previously, there is a large difference in the topography in the southern polar regions (figure 4). As will be shown later, this results in significantly weaker waves, both transient and stationary, in the southern winter hemisphere with the Consortium topography compared to the DTM. The stronger wave motions in the DTM case may be responsible for the increased dynamical warming, resulting in the observed differences in the zonal-mean fields. Differences are much smaller in the northern autumn and winter cases (figures 8 and 9) indicating that at these periods the zonal-mean atmospheric circulation is virtually insensitive to topography.

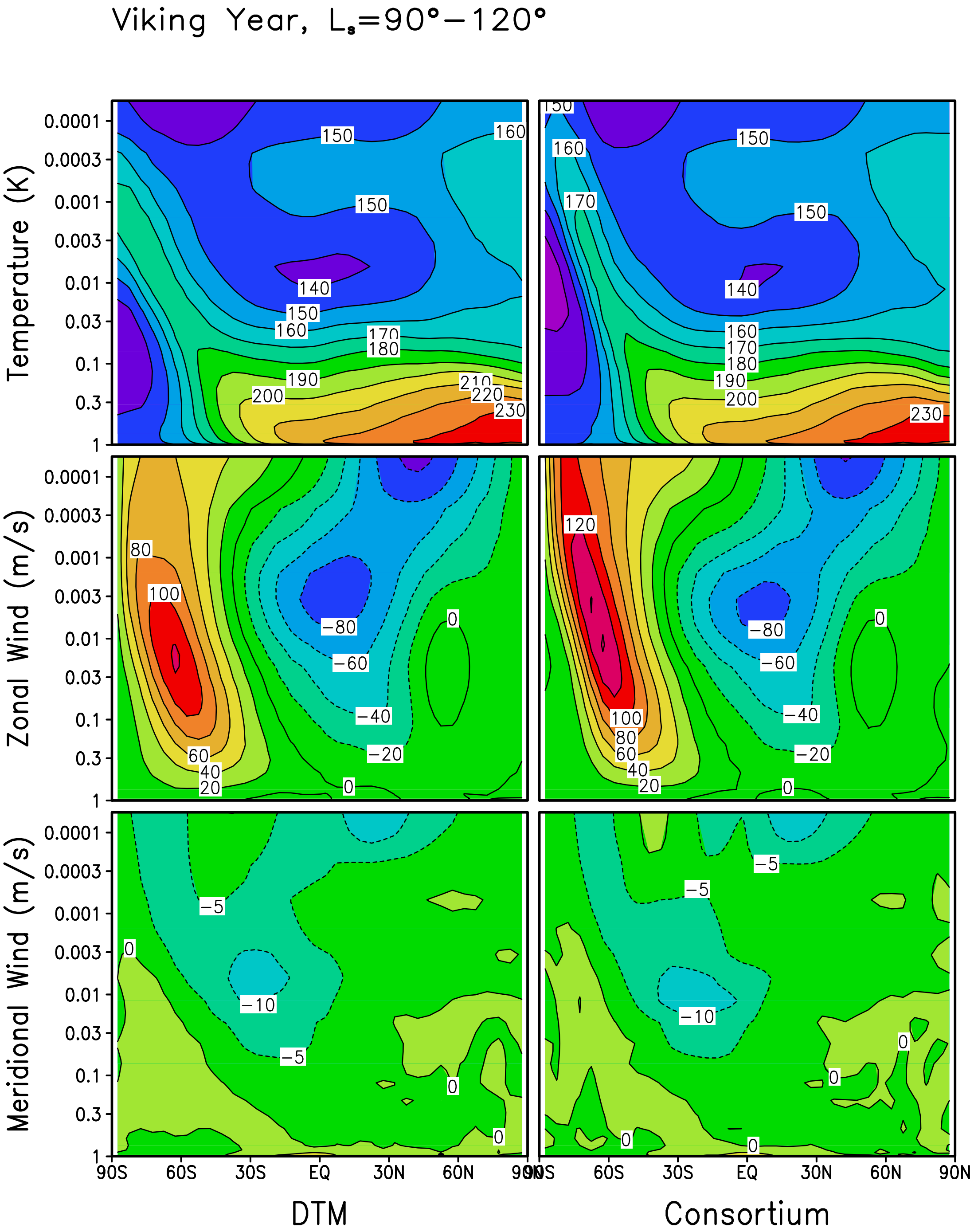

Figure 7: Zonal-mean plots of temperature, zonal and meridional wind from the DTM (left) and Consortium (right) experiments for northern hemisphere summer. The horizontal coordinate is latitude and the vertical is logσ, which is roughly proportional to altitude, ranging from the surface ($\sigma = 1$) to the model top boundary (approx. 100km).

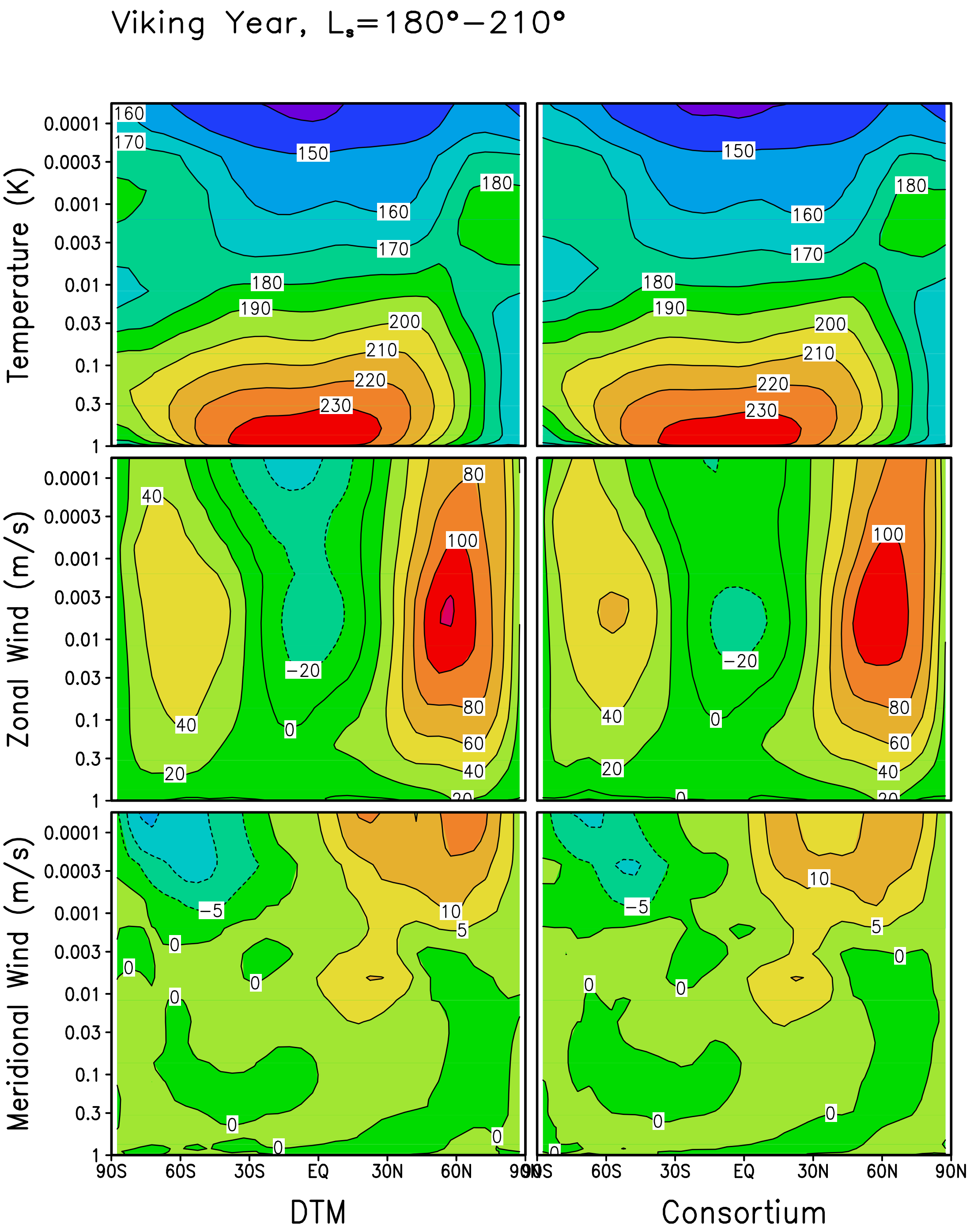

Figure 8: Zonal-mean plots, as in figure 7, for northern hemisphere autumn.

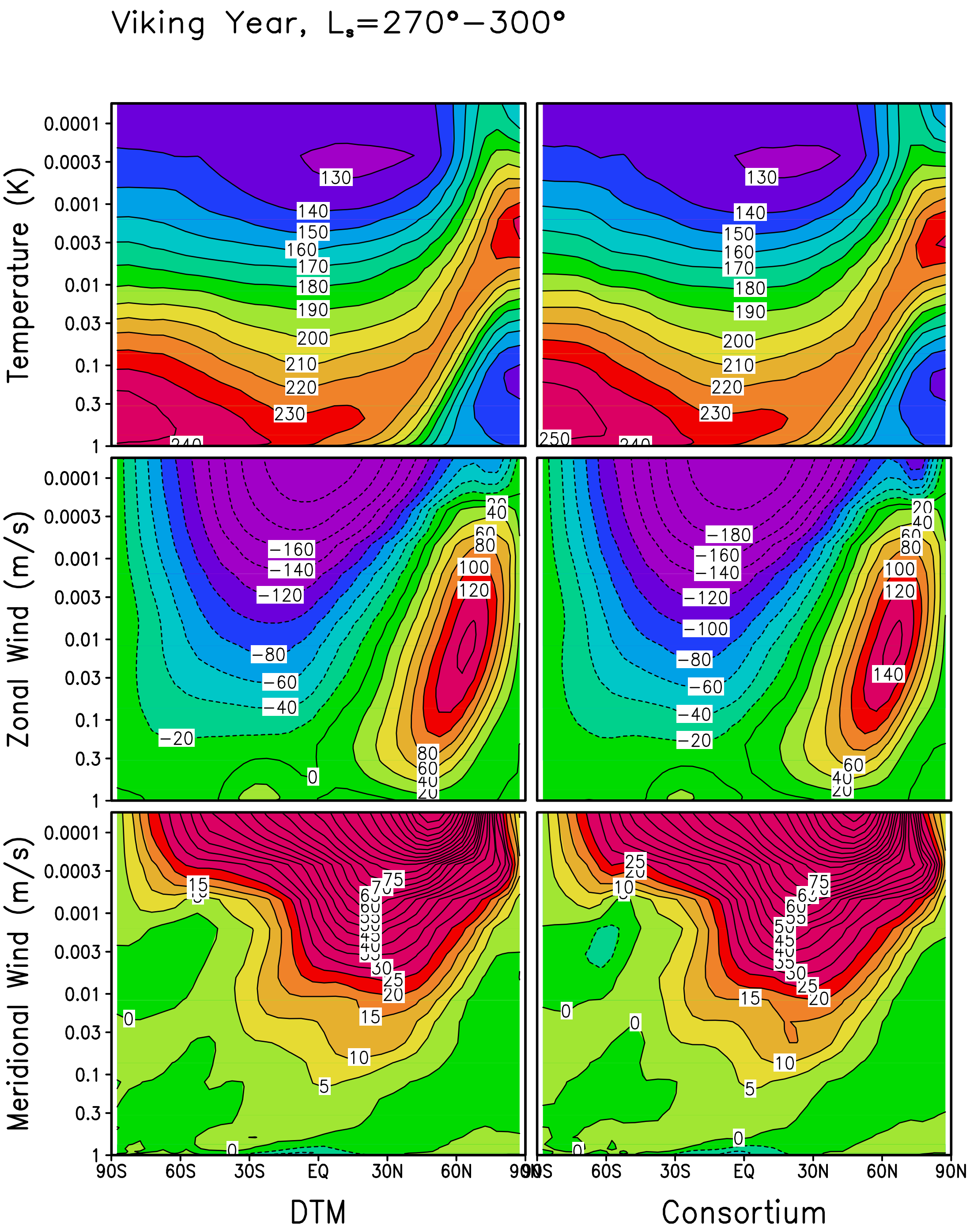

Figure 9: Zonal-mean plots, as in figure 7, for northern hemisphere winter.

3.2 Time-Mean Wind

Another important atmospheric variable, particularly when planning lander missions, is surface wind speed and direction. The time-mean, near-surface winds are compared in figures 10 and 11 for the DTM and Consortium experiments respectively. The wind fields appear to be more spatially coherent in the Consortium runs, presumably due to the smoother Consortium topography. Also there are considerable differences in regions where the wind flows are perpendicular to the topographic contours (slope winds), e.g. to the north of the Tharsis bulge where there are marked differences in the DTM and Consortium sets. It is also striking how weak the winds are near the southern pole during northern summer in the Consortium run compared to the DTM, again related to the difference in topography there. Surface wind therefore shows a strong sensitivity to the surface topography and the model simulation would benefit from a more accurate description of this field.

3.3 Diurnal Variability

The largest source of variability within each model season in most regions is as a result of the diurnal tide. To represent this cycle the Mars Climate Database stores means at 12 local times of day for each season [2, 4]. The sensitivity of this variability to the choice of topography is examined in this section using results from the northern hemisphere autumn season. The results from the other seasons are very similar.

In each case the martian solar day (sol) has been divided into 24 'hours' for convenience. Plots are shown at 6 'hour' intervals, labelled at the left of each plot with the local solar time which applies at 0° longitude, at the centre of each plot. In the first frame in each diagram the time is 00h, or midnight, at 0° longitude and midday at 180° longitude, and so on. The diurnal component of each variable is plotted, i.e. the mean value of that variable over the season at that local time of day with the diurnal-mean (the mean over all times of day) subtracted from it.

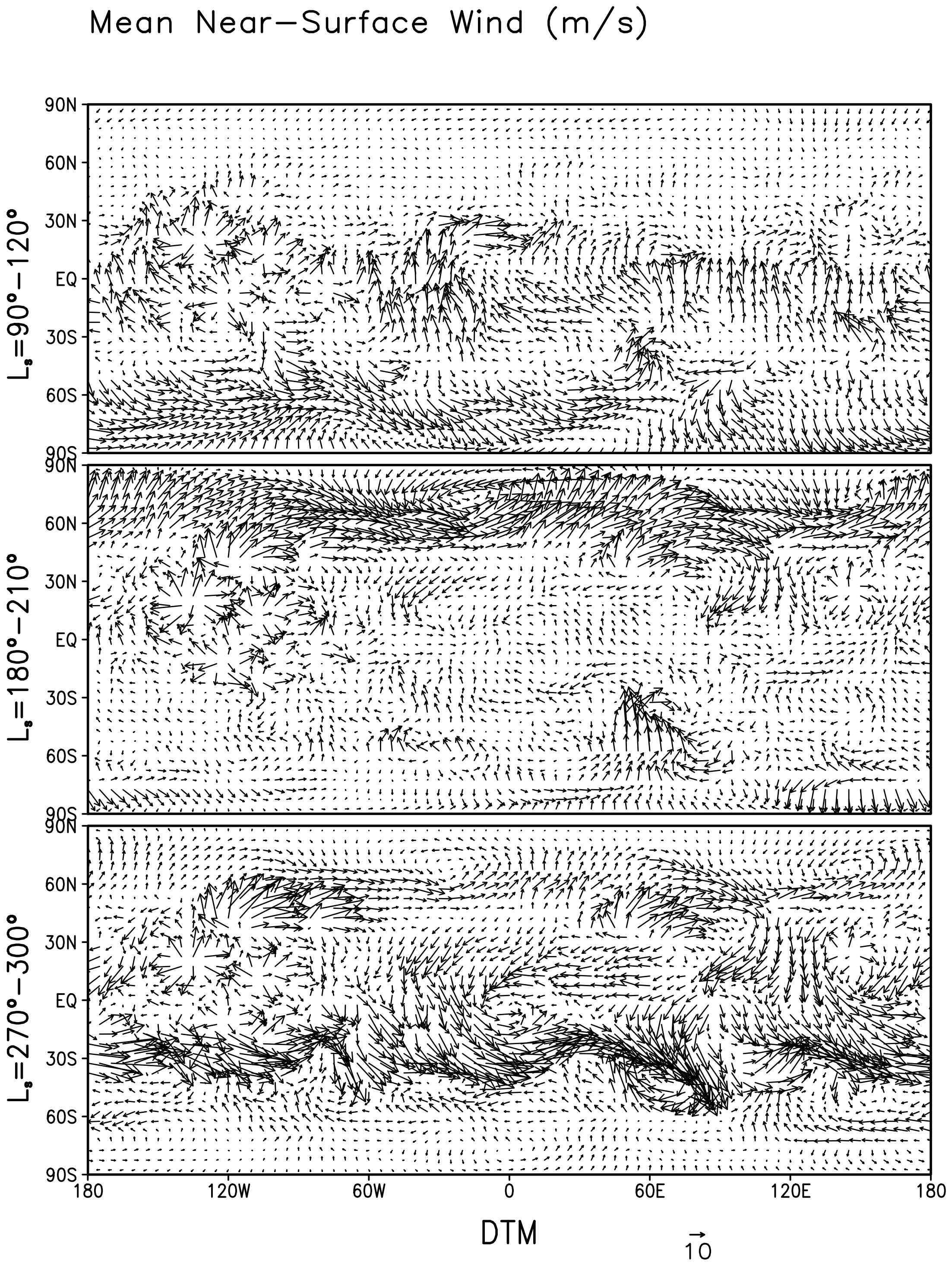

Figure 10: Time-mean near-surface ($\sigma = 0.9995$ or approx. 5m altitude) wind vectors for northern summer (top), autumn (middle) and winter (bottom) from the experiment with DTM topography. The scale vector is equivalent to 10m/s.

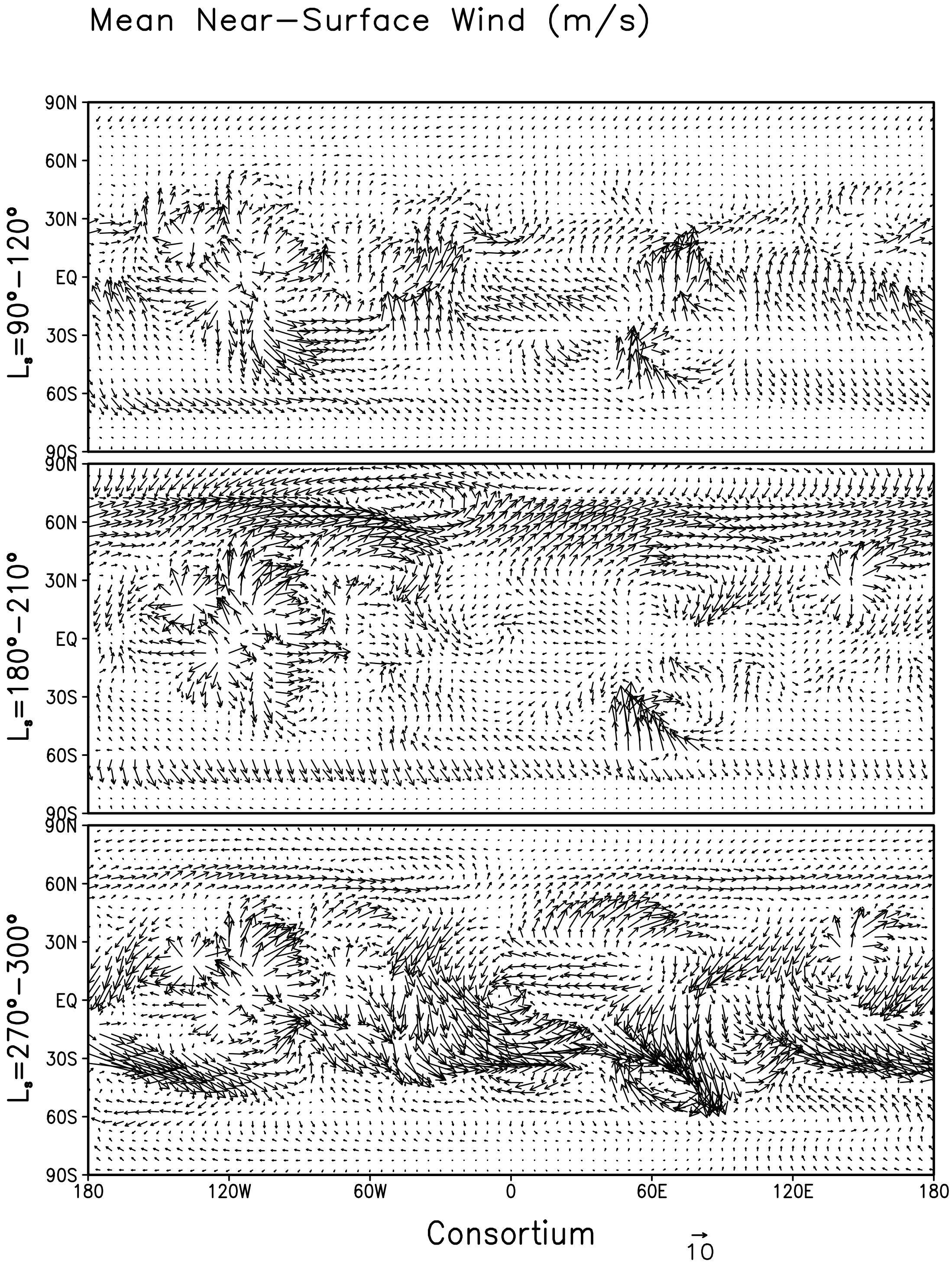

Figure 11: Near-surface wind vectors, as in figure 10, but for the experiment with Consortium topography.

3.3.1 Surface Temperature

The diurnal variation of surface temperature is largely determined by the diurnal cycle of insolation, the radiative transfer scheme and the maps of surface albedo and thermal inertia. Since these are the same in both experiments, except where the distribution of solid carbon dioxide ice on the ground differs, it is not surprising that the diurnal surface temperature fluctuations in both the DTM and Consortium experiment are very similar (figure 12). The difference between the two experiments is shown in figure 13 and is order 1 K or less over much of the surface. One exception is along a line near 60°S. This is close to the edge of the southern polar ice cap, which is subliming during this season. As can be seen in figure 12, the diurnal temperature fluctuations are much smaller over the ice in the polar region. Thus this difference in the diurnal temperature cycle may be ascribed to a difference in the position of the edge of the polar cap, which is itself related to the sharp 'cliff' and lower lying polar region in the southern hemisphere of the Consortium topography.

3.3.2 Surface Pressure

The thermal tide shown in the previous section, in combination with the surface topography, gives rise to a diurnal surface pressure tide in the atmosphere. This might be expected to show more differences than the thermal tide, since the topography in each experiment is different, even though the thermal forcing is similar. In fact, the diurnal surface pressure tide, also shows a remarkable insensitivity to choice of topography, as shown in figure 14. The difference between the experiments, shown in figure 15, is generally about 2 Pa, compared to a diurnal peak-to-peak variation of order 60 Pa. It should be noted that, although the diurnal variation in surface pressure in both experiments has a very similar form and amplitude, the mean surface pressure may differ by very large amounts (100 Pa or more, at any one point) between the two experiments, owing to the differences in the topographic height illustrated in figure 4.

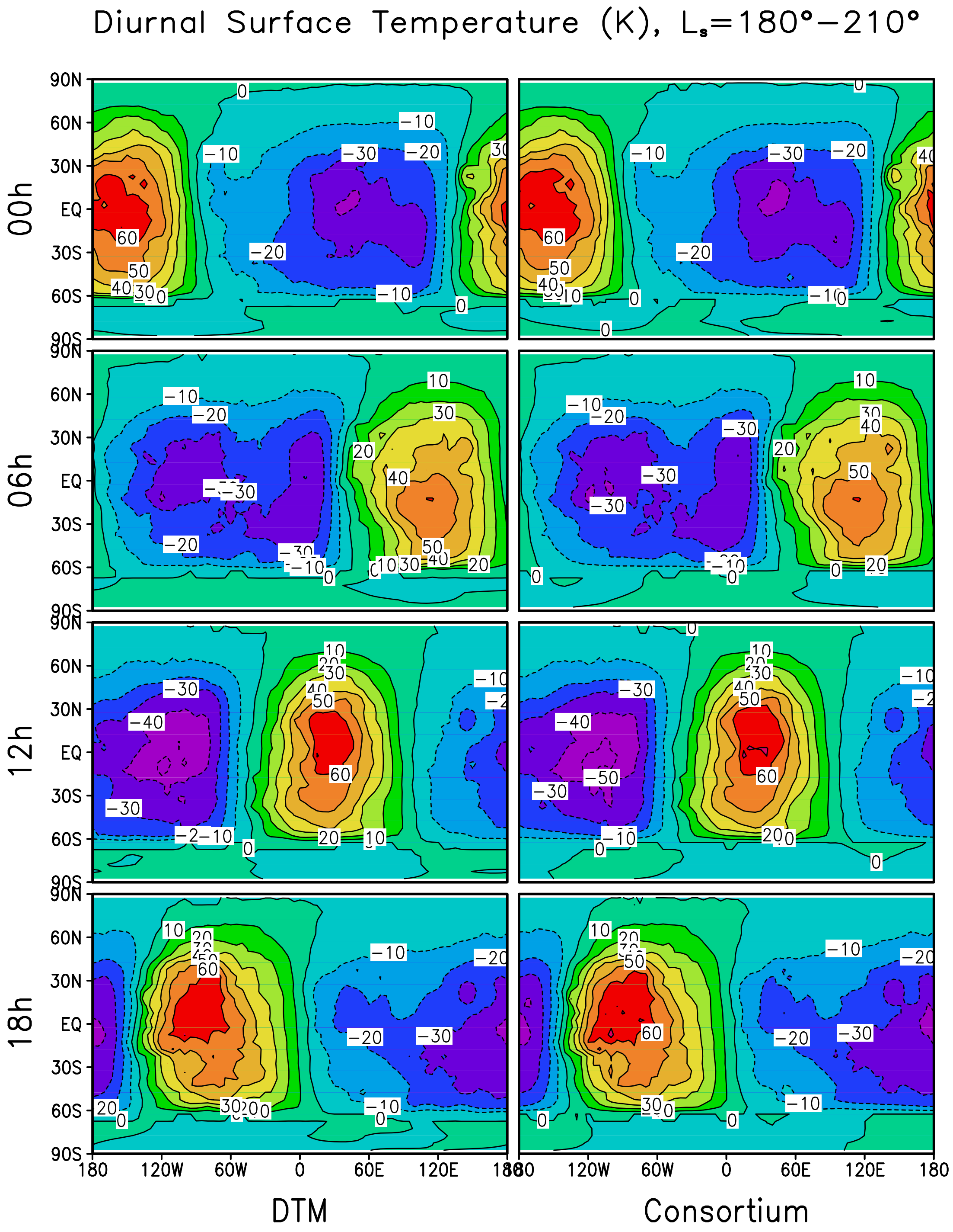

Figure 12: Seasonal-mean surface temperature maps for northern autumn at four times of day from the DTM (left) and Consortium (right) experiments. The diurnal-mean surface temperature has been subtracted in each case.

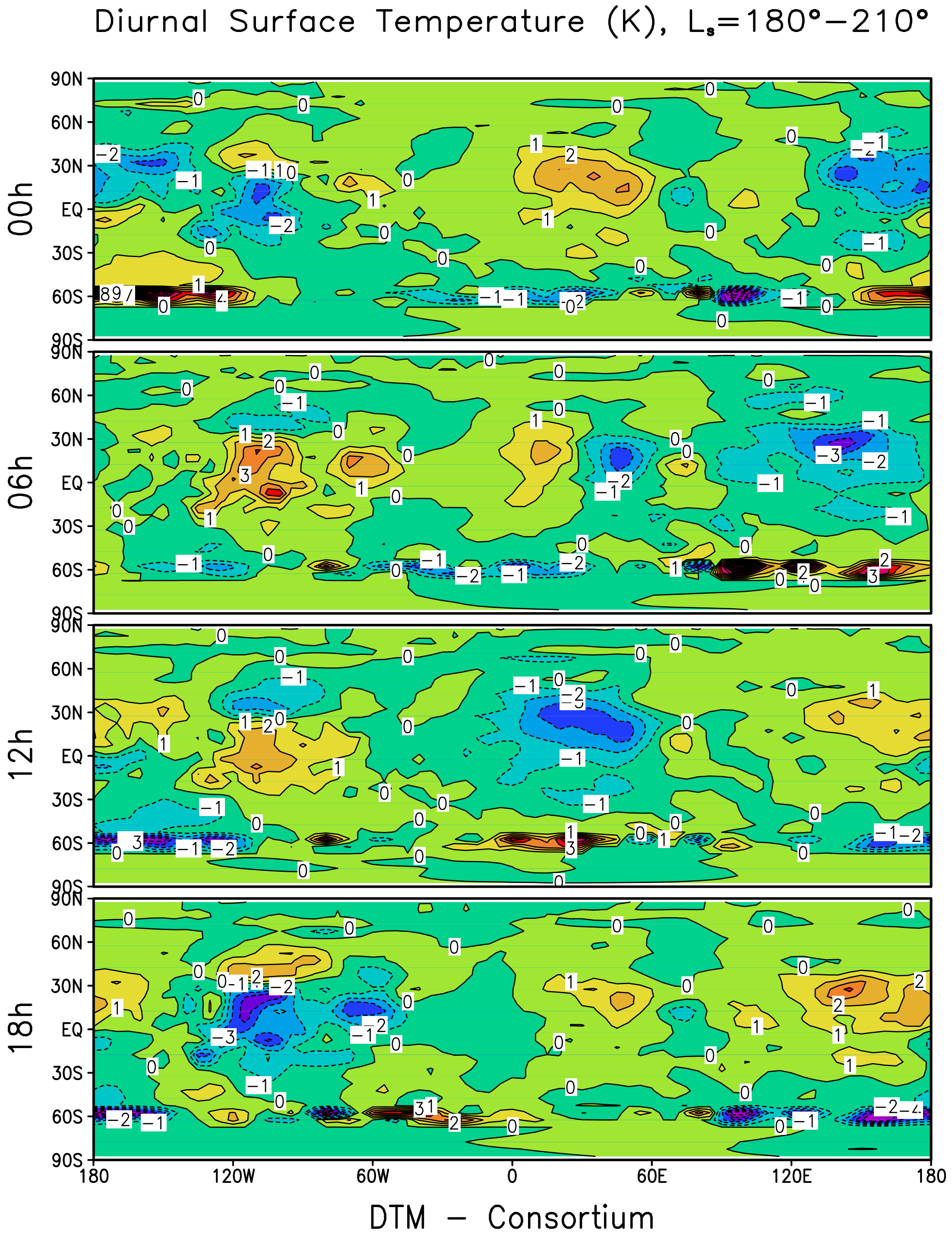

Figure 13: The difference, DTM - Consortium, between the diurnal surface temperatures shown in figure 12, with an expanded longitudinal scale.

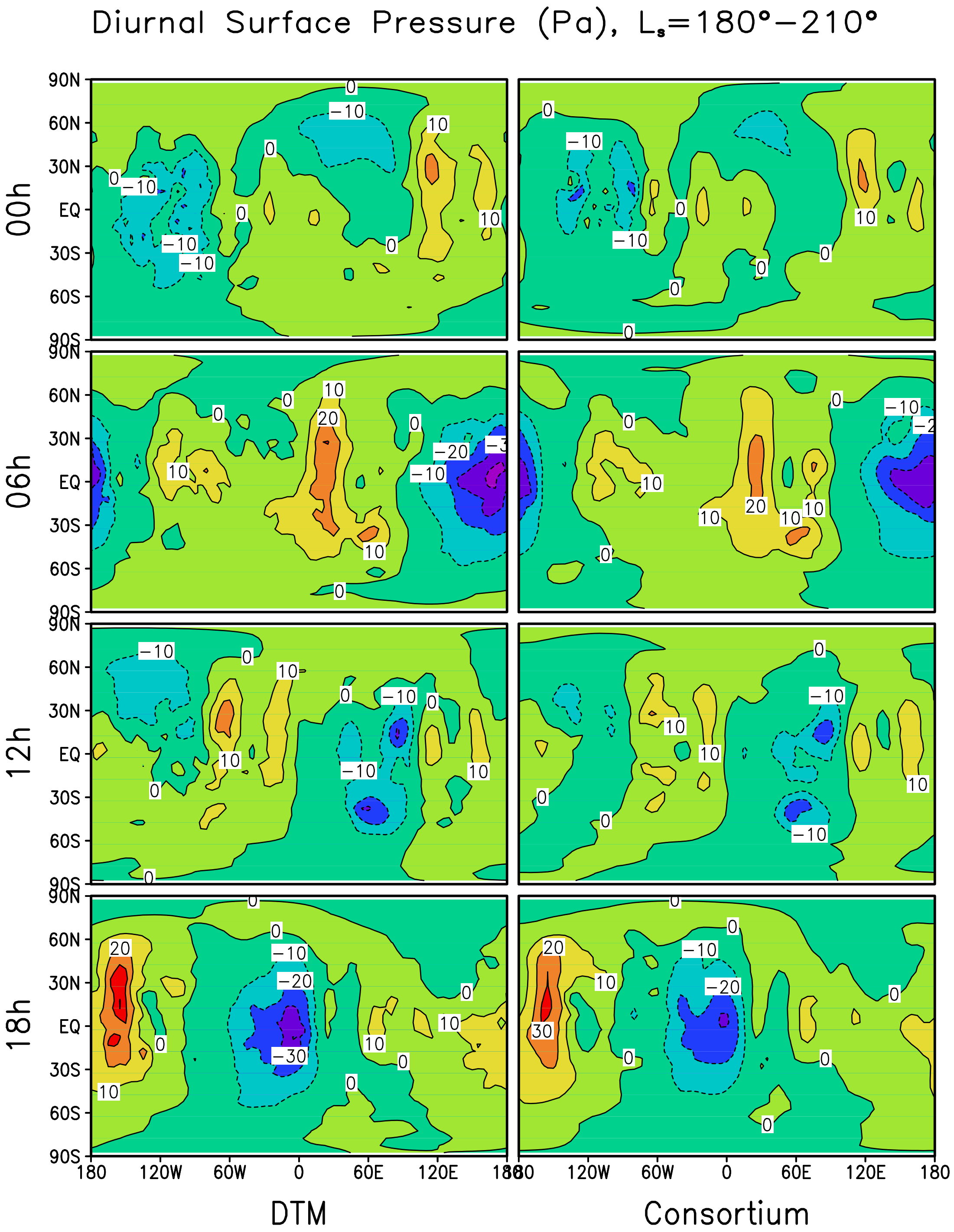

Figure 14: Seasonal-mean surface pressure maps for northern autumn at four times of day from the DTM (left) and Consortium (right) experiments. The diurnal-mean surface pressure has been subtracted in each case.

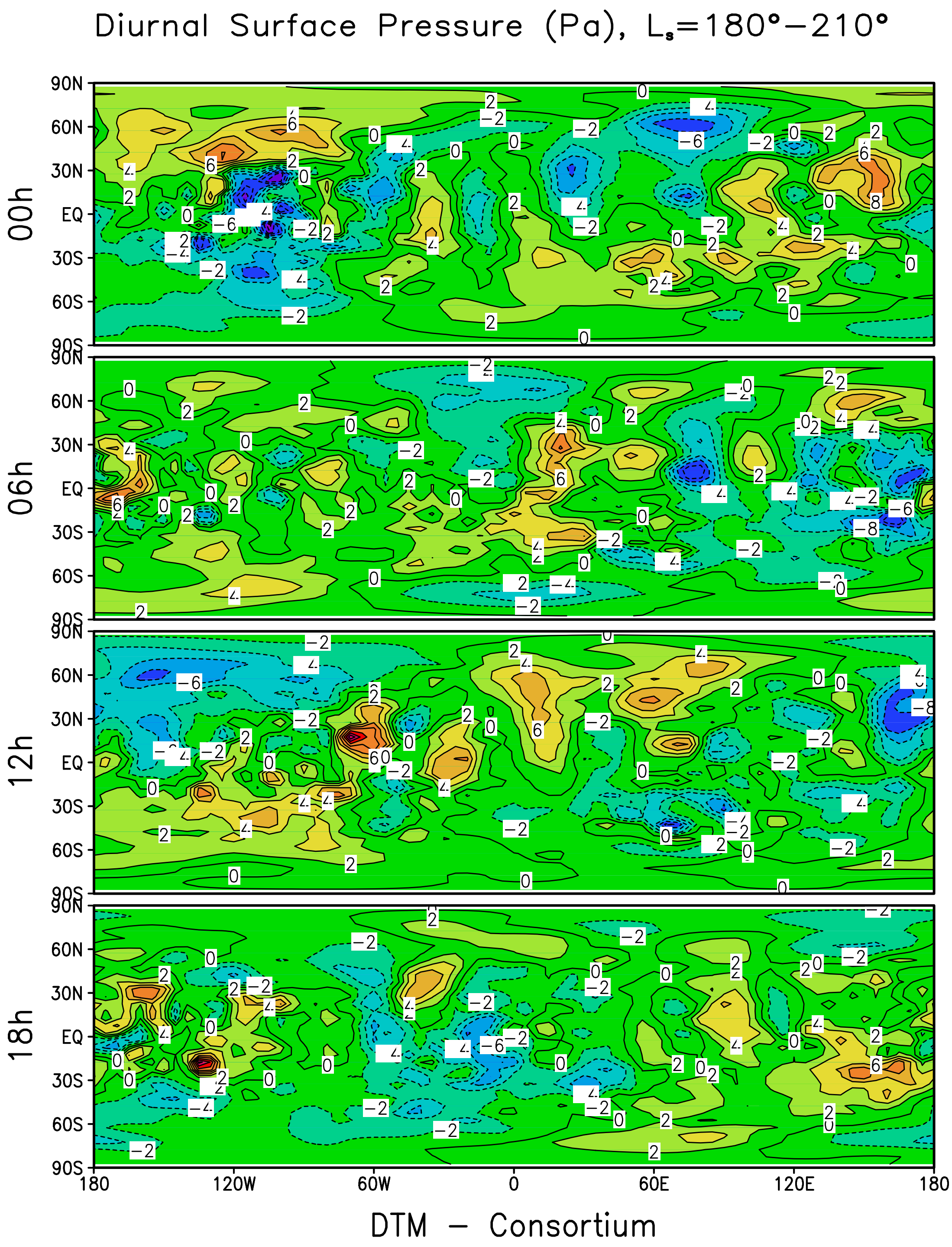

Figure 15: The difference, DTM - Consortium, between the diurnal surface pressures shown in figure 14, with an expanded longitudinal scale.

3.3.3 Near-Surface Wind

The diurnal component of the near-surface wind is shown in figure 16 for the DTM experiment, in figure 17 for the Consortium experiment and the difference between them is shown, with the same vector scale, in figure 18. Comparison with the time-mean winds at the same height, shown in figure 10, reveals that the diurnal component of the wind at this height is of order three times greater than the time-mean. Figure 18 also reveals that the difference between the diurnal winds with each topographic dataset is of the same order as the amplitude of the diurnal winds themselves. This is principally a result of differences in wind direction as a result of differences in local slopes and is particularly apparent near the Tharsis ridge in the northern hemisphere. The diurnal wind generally blows down-slope during the night and reverses to up-slope during the day. The details of the topography are therefore vital to determining the direction of the near-surface wind. If a prediction is required, an accurate topographic map is essential.

3.4 Transient Waves

Day-to-day fluctuations within a season, e.g. due to synoptic weather systems and other intra-seasonal changes, can be represented as a standard deviation about the mean at the same local time of day over the season. These standard deviations were calculated for each of the 12 local times of day used to represent the diurnal cycle and then averaged to give an estimation of the total component of variability due to transient behaviour.

Figure 19 shows this component of the surface pressure field at each season for each topography experiment. In each case the region of largest variability is at high latitudes in the winter hemisphere, near the edge of the polar cap. In both cases the variability in the southern winter (first frame) is about half the amplitude of the variability in the northern winter (third frame) and is also more symmetric in longitude. The autumn season also shows most transient activity in the northern hemisphere, with only a very weak maximum near the south pole. These regions correspond to 'storm tracks' along which planetary waves are propagating. The differences between the DTM and Consortium in

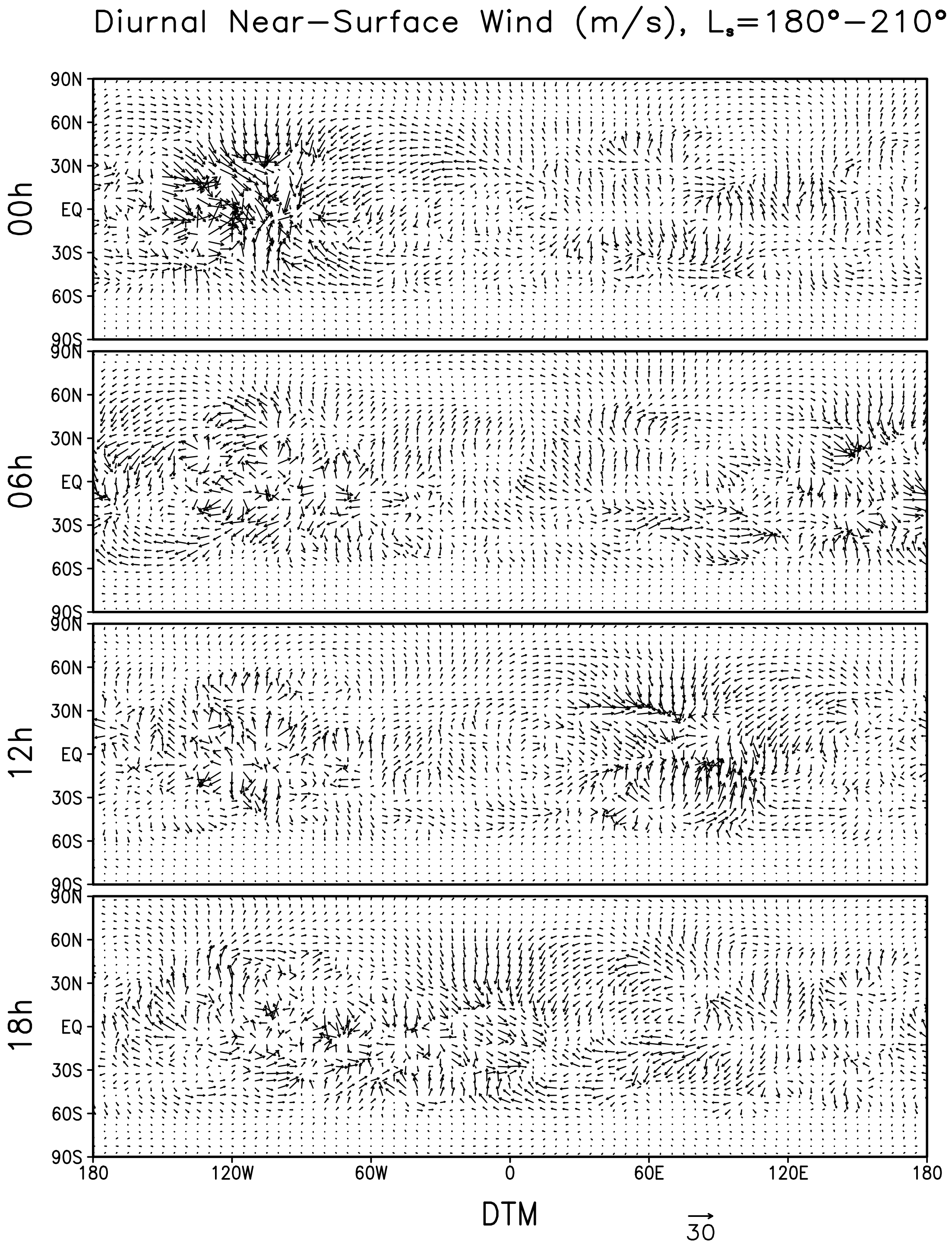

Figure 16: The diurnal component of the near-surface ($\sigma = 0.9995$ or approx. 5m altitude) wind vectors at four times of day for northern autumn from the experiment with DTM topography. The diurnal-mean wind (figure 10, second frame) has been subtracted in each case. The scale vector is equivalent to 30m/s.

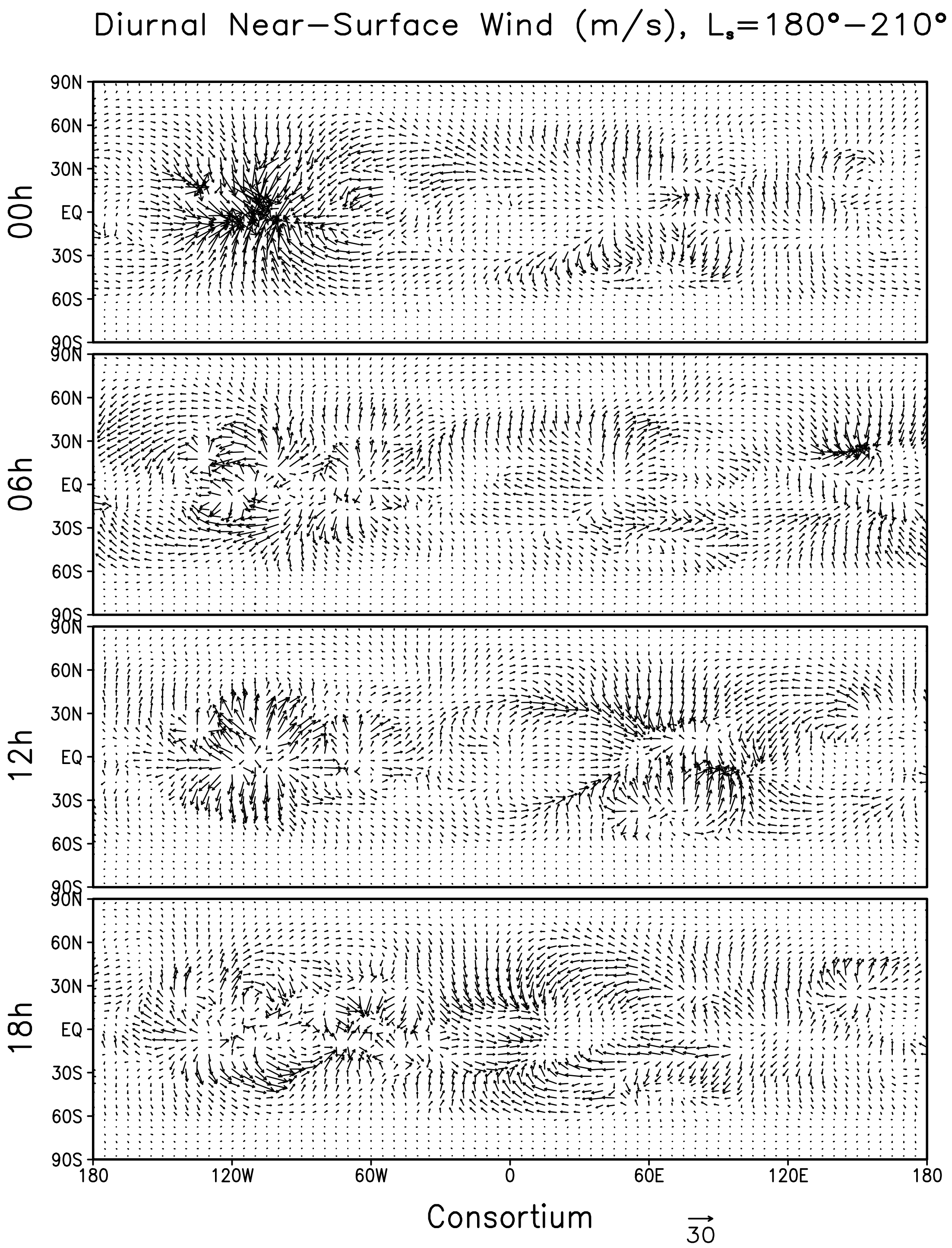

Figure 17: Diurnal component of the near-surface wind, as in figure 16, but for the experiment with Consortium topography.

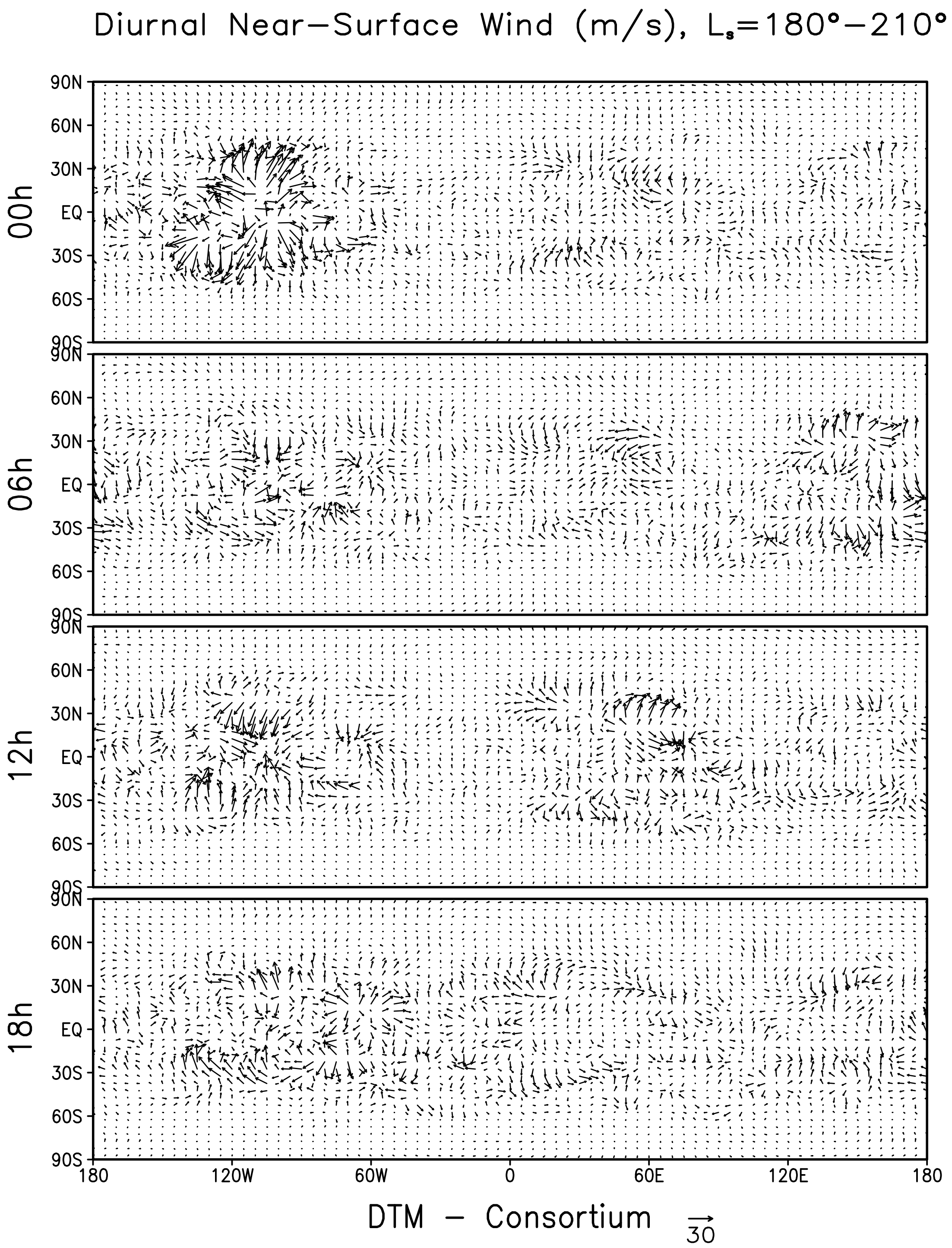

Figure 18: The difference, DTM - Consortium, between the diurnal near-surface winds shown in figures 16 and 17.

transient behaviour are often small, with the most notable exception being the 'storm track' in northern winter which is clearly divided into two strong maxima in the case of the DTM, but which has only one clear maximum in the Consortium experiment (and also has a reduced amplitude very near the pole in the Consortium where the topography rises). This is a result of the increased longitudinal wavenumber two characteristic of the DTM topography in northern mid-latitudes, owing to the extension northwards of the Tharsis ridge compared to the Consortium data.

The latitude-height form of the transient behaviour may be examined by plotting the zonal-mean of the time-mean standard deviation. Figure 20 shows this for three seasons for each topography experiment for the meridional (south-north) wind. Plots of other variables such as zonal wind and temperature show a similar form, e.g. [7]. It can be seen that, as in the surface pressure signature (figure 19), transient behaviour is strongest in the winter hemisphere at high latitudes, and particularly so in the northern winter hemisphere. During northern winter there appears to be little sensitivity to topography (figure 20, third frame). However, in the southern winter (figure 20, first frame) the transients appear to be about twice as strong in the DTM experiment close to the ground, again related to the different zonal-mean slopes in the topographies in this region with a rise to a high south pole in the DTM and an abrupt fall to a flat, low south pole in the Consortium topography (figure 4). Higher in the atmosphere, the variability is comparable in both experiments. The variability during the autumn equinox season (figure 20, second frame) is very similar in the two experiments over most of the atmosphere, but with one interesting area of difference in the region of high variability which extends downwards between 60°N and 90°N; this is only about two thirds as strong in the DTM experiment as it is in the Consortium experiment. The reason for this is not clear at present, though the precise values in this region at equinox are sensitive to the averaging period chosen.

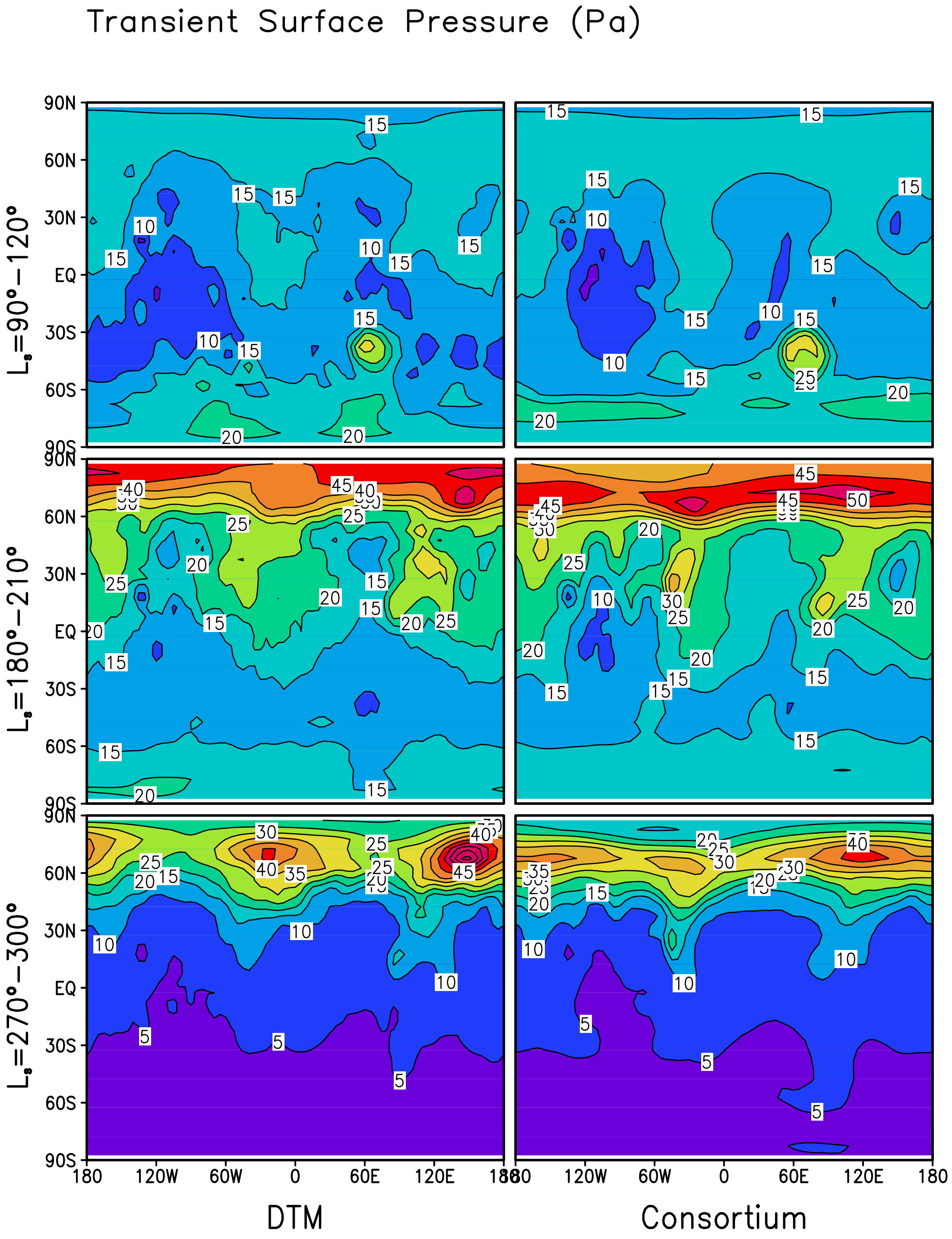

Figure 19: The time-mean of the transient (variability other than diurnal) surface pressure field from the DTM (left) and Consortium (right) experiments for northern hemisphere summer (top), autumn (middle) and winter (bottom).

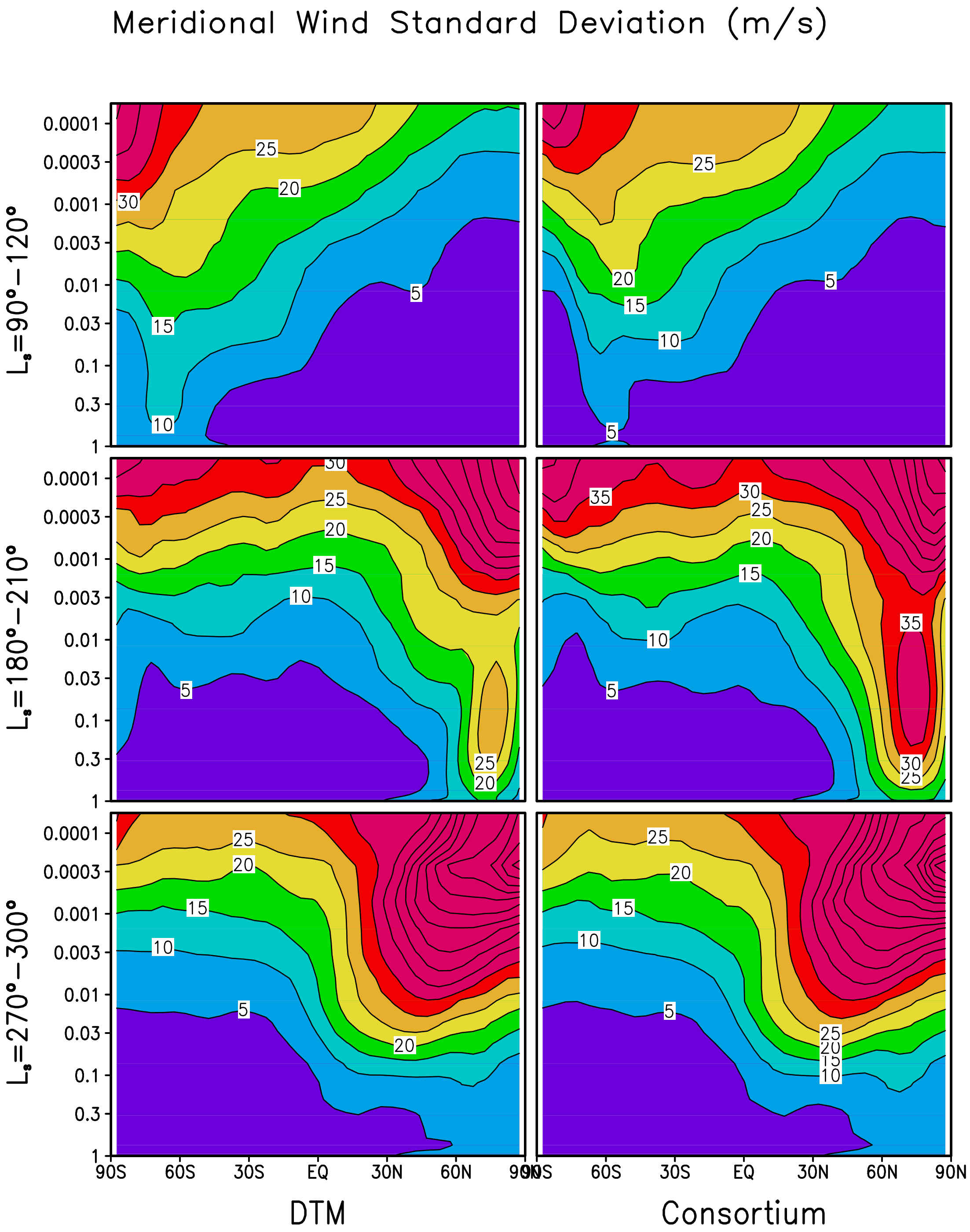

Figure 20: The time-mean, zonal-mean standard deviation of the meridional wind from the DTM (left) and Consortium (right) experiments for northern hemisphere summer (top), autumn (middle) and winter (bottom).

3.5 Stationary Waves

One feature of the circulation that is likely to be sensitive to the surface topographic data is the stationary wave behaviour. Stationary waves are planetary scale wave-like features that generally have their largest amplitudes at high levels, see e.g. [1]. Differences in the large scale characteristics of the DTM and Consortium sets could affect both the amplitude, phase and wavenumber of the stationary waves. Figure 21 shows the time-mean meridional wind on the $\sigma = 0.123568$ surface, approximately 21km above the ground, for three seasons from the DTM and Consortium experiments. This diagnostic highlights the stationary wave behaviour well.

During southern winter, the DTM integration shows a slightly larger amplitude stationary wave compared to the Consortium case. Such differences may contribute to the differences in jet structure seen in figure 7 via nonlinear interactions with the mean flow (see, e.g. [1] for a more detailed explanation of this mechanism). During northern winter, there is a strong wavenumber two pattern in the DTM run, while the Consortium run again shows a lower amplitude feature of about the same scale. The most marked difference occurs during the autumn period when the DTM shows a strong wavenumber two wave near the north pole and a clear wavenumber one near the south pole, whereas the Consortium experiment has a weaker wavenumber one disturbance near the north pole and no clear stationary wave in the south. These results are comparable with linear modelling studies using both the Consortium [6] and DTM [9] which both also predict that wavenumber one and two stationary waves will be present in the winter hemisphere, though they do not describe flows for the equinox period.

Despite the subtle, and important, differences in stationary wave behaviour with each topographic dataset, it is worth noting that the differences in meridional wind are reasonably small over most of the atmosphere. Typically, these differences are of order 1 m/s and only reach 5 m/s or greater near the polar regions where the waves are strongest. This is much smaller than the diurnal variability in each experiment and comparable to, or smaller than, the variability resulting from transient waves (see figure 20). Thus, while stationary waves can be of importance in polar regions at some times of year, they may not result in very strong sensitivity to topography for many applications, especially in the region 45°N–45°S where their effect is negligible.

3.6 Density Profiles

The density of the martian atmosphere is one of the most important variables used by engineers in mission planning, e.g. when calculating entry trajectories or aerobraking manoeuvres. Here we compare various vertical profiles of density from the DTM and Consortium runs from southern and northern winter, as might be done with the Martian Climate Database in practice.

Because density varies logarithmically with height it is useful to compare any density profile with some 'standard' profile. Figure 22 shows the northern hemisphere COSPAR standard atmospheric density profile from the surface to approximately 90 km. All density profiles are referenced to this profile by expressing the density as a percentage difference, d, from the COSPAR profile,

$$d = 100 * \frac{\rho_{COSPAR} - \rho}{\rho_{COSPAR}}. \tag{1}$$

We show profiles at four points on the planet, longitude 50°W, latitude 22.5°N (model grid-point nearest to the Viking Lander 1 site), longitude 225°W, latitude 47.5°N (model grid-point nearest to the Viking Lander 2 site), longitude 50°W, latitude 22.5°S and longitude 225°W, latitude 22.5°S (the last two are the corresponding points in the southern hemisphere).

Figures 23 and 24 compare the density profiles (middle curves) from the DTM and Consortium runs using the method described above. Also shown, as the the curves either side of the mean, are the mean profiles ± one standard deviation of density (including the diurnal component). There is very little difference between the DTM and the Consortium profiles of density and where there are slight differences in the mean profiles the variations are very much less than the one standard deviation curves. Hence density above the surface is insensitive to the choice of surface topography, at least in all the cases tried.

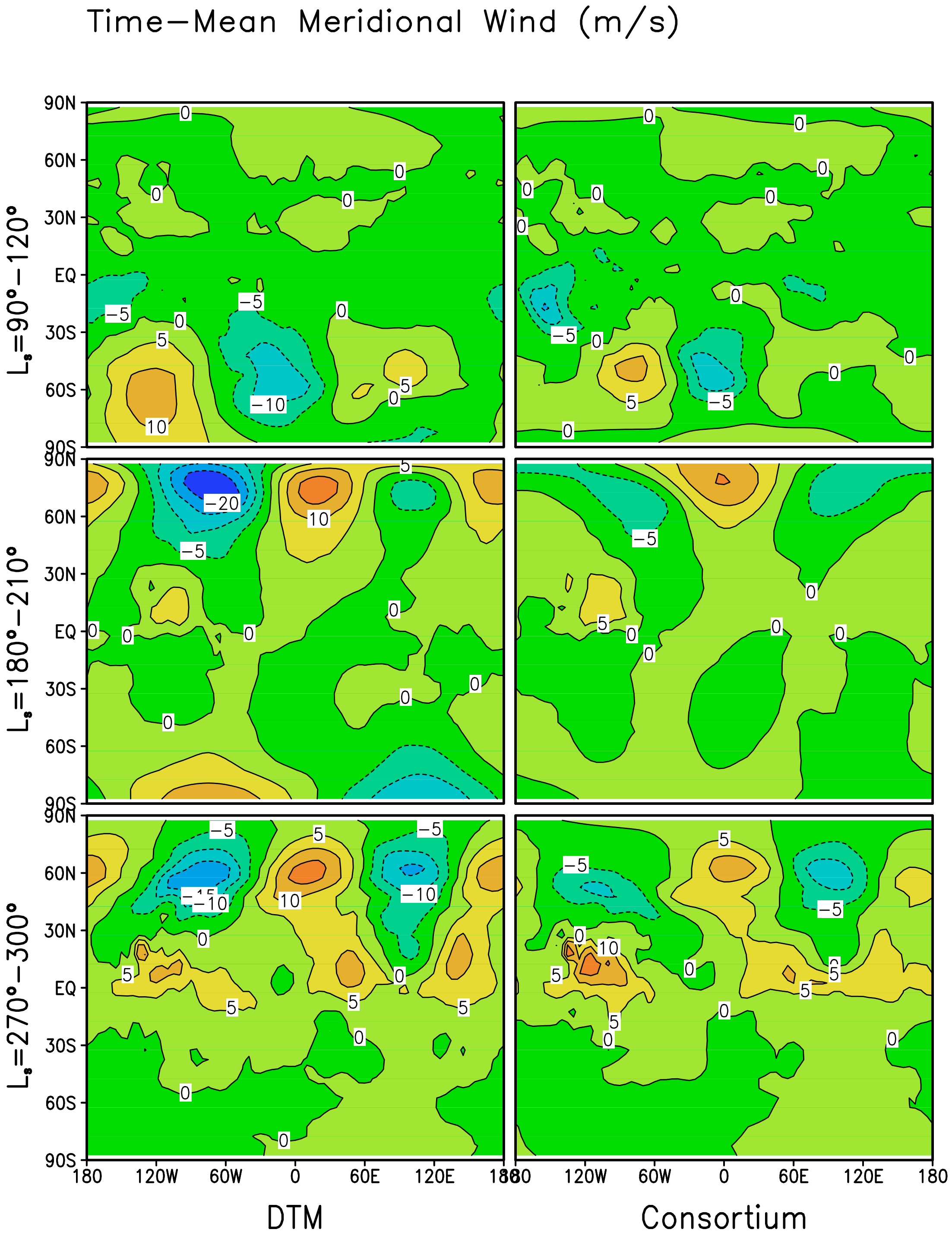

Figure 21: The time-mean meridional wind on the $\sigma = 0.123568$ surface (approx. 21 km altitude) from the DTM (left) and Consortium (right) experiments for northern hemisphere summer (top), autumn (middle) and winter (bottom).

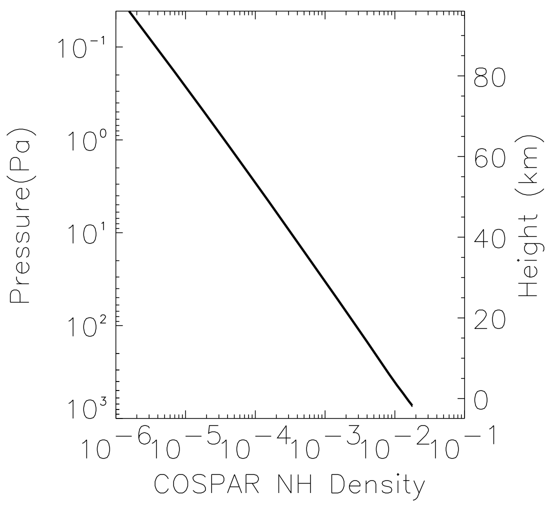

Figure 22: COSPAR Northern Hemisphere mean density for Mars. Note the logarithmic scale on the abscissa.

4 Summary

Model integrations with the two commonly used topographic datasets, the DTM and Consortium, show a broad agreement between them in many atmospheric fields indicating no major sensitivity of the circulation to the current uncertainty in topographic height. Vertical profiles of temperature and density are particularly insensitive in most cases. The differences between the model integrations with each topographic dataset are much smaller than the intrinsic variability in each case, and, in fact, generally smaller than the differences between two different atmospheric models run with the same topographic dataset [7]. The form and amplitude of the major sources of variability were also found to be similar with each topography. This is particularly so in the equatorial and mid-latitude regions where there was very little difference between the experiments. The greatest differences in the variability were to be found at high latitudes in the winter hemisphere. The current Mars Climate Database may therefore be regarded as producing useful results in most cases, despite the uncertainty in the martian surface topography.

There are however some differences in the model runs which must be resolved in

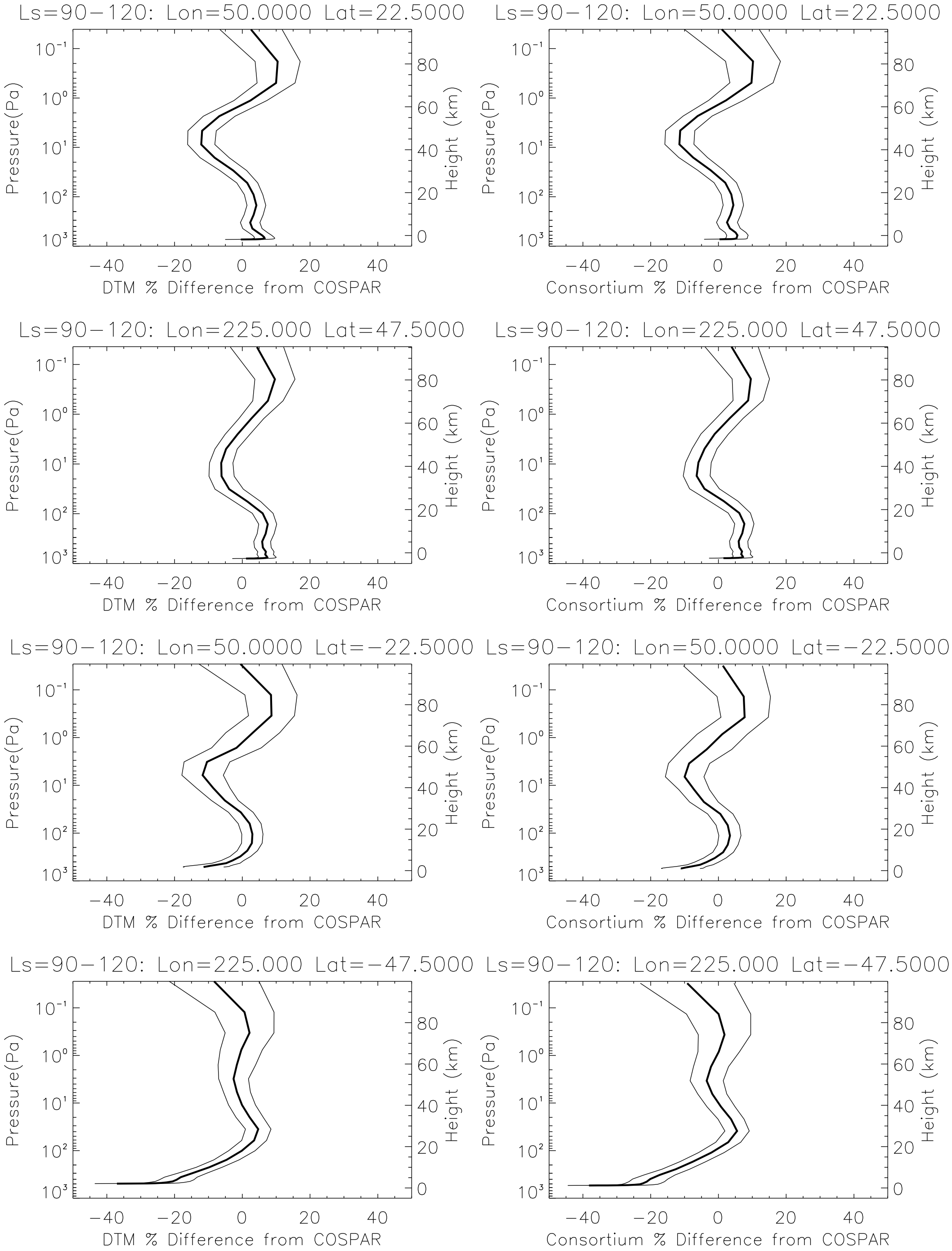

Figure 23: A comparison of density profiles (expressed as % differences from the COSPAR standard atmosphere) from model runs at $L_s = 90° - 120°$, using the Viking dust scenario and with the DTM (left) or Consortium (right) topography. The central curve is the mean and the curves either side are one standard deviation away.

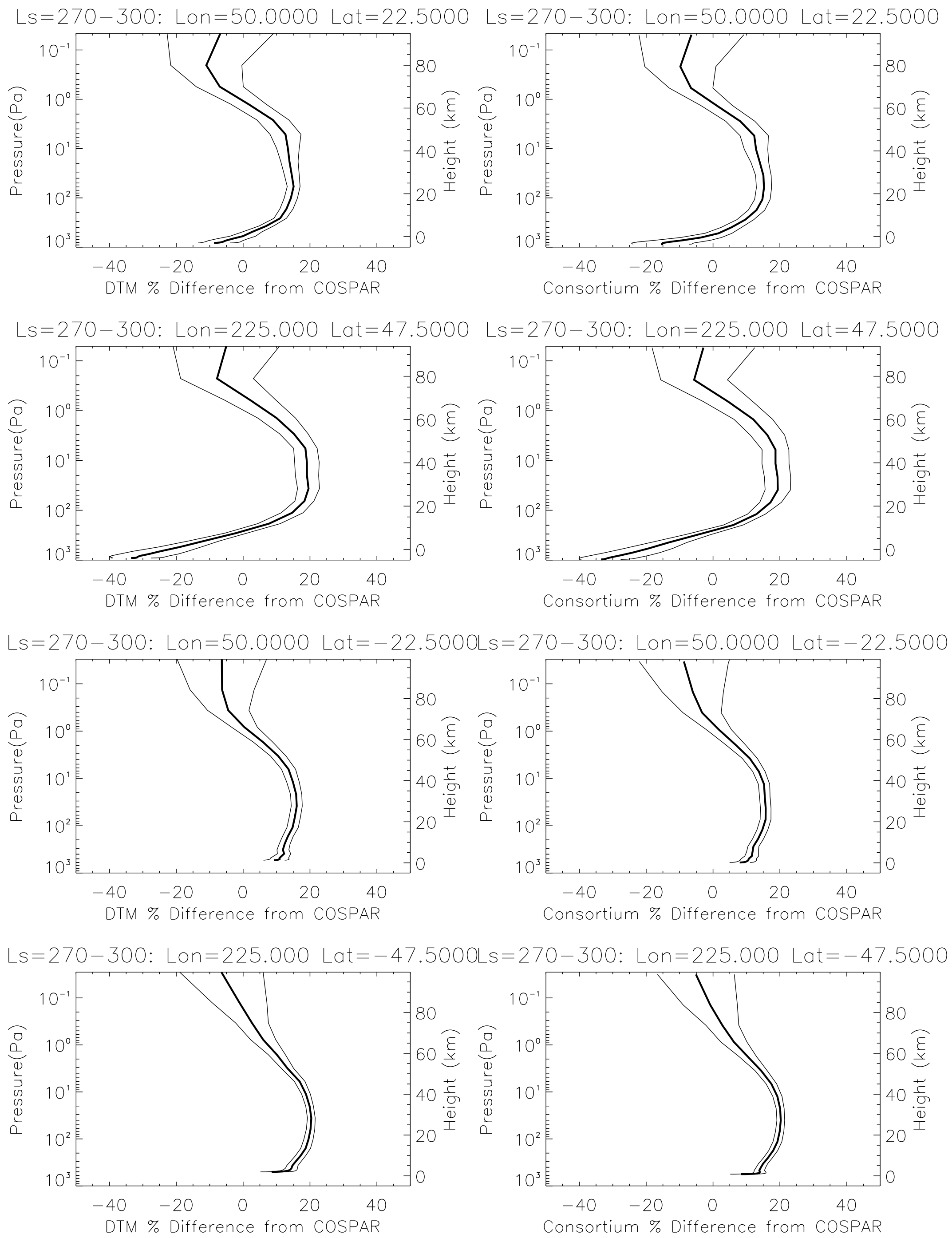

Figure 24: A comparison of density profiles (expressed as % differences from the COSPAR standard atmosphere) from model runs at $L_s = 270° - 300°$, using the Viking dust scenario and with the DTM (left) or Consortium (right) topography. The central curve is the mean and the curves either side are one standard deviation away.

order to produce a more accurate simulation of the atmosphere of Mars. In particular, if a prediction of mean surface pressure or near-surface wind amplitude and, especially, direction is required, then the choice of topographic dataset is vital. A more authoritative climate simulation in these respects will only be attainable when the Laser Altimeter (MOLA), onboard the Mars Global Surveyor (MGS) spacecraft, returns an accurate topographic map. Owing to the current problems with the MGS orbital insertion, this map is now unlikely to become available until late in 1999. Once this data has been processed and validated it will certainly be a worthwhile exercise to re-compile the Mars Climate Database with results from runs conducted using the new topographic map.

References

[1] D. G. Andrews, J. R. Holton, and C. B. Leovy.
Middle Atmosphere Dynamics.
Academic Press, 1987.

[2] M. Collins, S. R. Lewis, P. L. Read, N. P. J. Thomas, O. Talagrand, F. Forget, R. Fournier, F. Hourdin, and J-P Huot.
A climate database for the martian atmosphere.
ESA Special Publication, SP-392:323–327, 1996.

[3] M. Collins, S. R. Lewis, and P. L. Read.
Gravity wave drag in a global circulation model of the martian atmosphere: Parameterisation and validation.
Adv. Space Res., 19:1245–1254, 1997.

[4] M. Collins, S. R. Lewis, and P. L. Read.
Mars Climate Database v1.0: Detailed design document.
ESA Technical Report, 1997.

[5] E. J. Christensen.
Martian topography derived from occultation, radar, spectral, and optical measurements.

J. Geophys. Res., 80:2909–2913, 1975.

[6] J. L. Hollingsworth, and J. R. Barnes.
Forced stationary planetary waves in Mars's winter atmosphere.
J. Atmos. Sci., 53:428–448, 1996.

[7] F. Hourdin, C. Hourdin, and S. R. Lewis.
Technical note on studies of model differences.
ESA Technical Report, 1998.

[8] G. F. Lindal, H. B. Hotz, D. N. Sweetnam, Z. Shippony, J. P. Brenkle, G. V. Hartsell, R. T. Spear, and W. H. Micheal.
Viking radio occultation measurements of the atmosphere and topography on Mars.
J. Geophys. Res., 84:8443–8456, 1979.

[9] L. Nayvelt, P. J. Gierasch, and K. H. Cook.
Modeling and observations of martian stationary waves.
J. Atmos. Sci., 54:986–1013, 1997.

[10] USGS–NASA.
Mission to Mars: Digital Topographic Map.
USA–NASA–PDS–VO–2007, Version 2, 1993.

[11] S. S. C. Wu.
A method of defining topographic datums of planetary bodies.
Annal. Geophys., 1:147–160, 1981.